Gadolinium tissue deposition in the periodontal ligament of mice with reduced renal function exposed to Gd-based contrast agents

Riccarda Delfino[a], Matteo Biasotto[b], Riccardo Candido[c], Matteo Altissimo[d], Marco Stebel[e], Murielle Salomè[f], Johannes T. van Elteren[g], Katarina Vogel Mikuš[h,i], Cristina Zennaro[b], Martin Šala[g], Riccardo Addobbati[j], Giuliana Tromba[d], Lorella Pascolo[j,*]

[a] Department of Chemical and Pharmaceutical Sciences University of Trieste, Italy
[b] Department of Medicine, Surgery and Health Sciences, University of Trieste, Italy
[c] University Hospital Trieste, Italy
[d] Sincrotrone Trieste S.C.p.A, Trieste, Italy
[e] Department of Life Sciences, University of Trieste, Trieste, Italy
[f] European Synchrotron Radiation Facility, Grenoble, France
[g] Department of Analytical Chemistry, National Institute of Chemistry, Ljubljana, Slovenia
[h] Biotechnical faculty, University of Ljubljana, Ljubljana, Slovenia
[i] Jozef Stefan Institute, Ljubljana, Slovenia
[j] Institute for Maternal and Child Health, IRCCS Burlo Garofolo, Trieste, Italy

ARTICLE INFO

Keywords:
Gadolinium
MRI contrast agent
GBCAs
Periodontal ligament
XRF
5/6 nephrectomy

ABSTRACT

Gadolinium deposition in tissue is linked to nephrogenic systemic fibrosis (NSF): a rare disorder occurring in patients with severe chronic kidney disease and associated with administration of Gd-based contrast agents (GBCAs) for Magnetic Resonance Imaging (MRI). It is suggested that the GBCAs prolonged permanence in blood in these patients may result in a Gd precipitation in peripheral or central organs, where it initiates a fibrotic process. In this study we investigated new sites of retention/precipitation of Gd in a mouse model of renal disease (5/6 nephrectomy) receiving two doses (closely after each other) of a linear GBCA. Two commercial GBCAs (Omniscan® and Magnevist®) were administered at doses slightly higher than those used in clinical practice (0.7 mmol/kg body weight, each). The animals were sacrificed one month after the last administration and the explanted organs (kidney, liver, femur, dorsal skin, teeth) were analysed by X-ray fluorescence (XRF) at two synchrotron facilities. The XRF analysis with a millimetre-sized beam at the SYRMEP beamline (Elettra, Italy) produced no detectable levels of Gd in the examined tissues, with the notable exception of the incisors of the nephrectomised mice. The XRF analyses at sub-micron resolution performed at ID21 (ESRF, France) allowed to clearly localize Gd in the periodontal ligaments of teeth both from Omniscan® and Magnevist® treated nephrectomised mice. The latter results were further confirmed by laser ablation inductively coupled plasma mass spectrometry (LA-ICP-MS). The study prompts that prolonged permanence of GBCAs in blood may result in Gd retention in this particular muscular tissue, opening possibilities for diagnostic applications at this level when investigating Gd-related toxicities.

1. Introduction

Gadolinium-based contrast agents (GBCAs) are extremely important diagnostic drugs formulated to have a rapid clearance upon administration, which assures an innocuous use in MRI procedures. However, in the last ten years important concerns on the safety of GBCAs have been raised (Tedeschi et al., 2017). The most important warning comes from the discovery of Nephrogenic Systemic Fibrosis (NSF) linked to GBCAs administration (Cowper et al., 2007). NSF was first recognized in 1997 in 15 dialyzed patients and described for the first time in 2000 (Cowper et al., 2000). This rare and invalidating disorder is characterized by fibrosis of the skin and connective tissues, with dermal lesions usually distributed symmetrically, developing on the trunk and extremities. Some specific signs have been described: cutaneous thickening of the skin with or without pigment alterations, swelling, progressive skin indurations, pruritus and burning sensations. The clinical

* Corresponding author at: Institute for Maternal and Child Health, IRCCS Burlo Garofolo, 34027, Trieste, Italy.
E-mail address: lorella.pascolo@gmail.com (L. Pascolo).

Accepted 22 November 2018

course of NSF can be progressive, frequently involving internal organs, and may even have a fatal outcome. NSF always occurs in patients with severe or end-stage chronic kidney disease, requiring dialysis (Galan et al., 2006).

Although the aetiology of NSF is currently unknown and considered multifactorial, evidence indicates that NSF development is undoubtedly linked to intravenous administration (i.v.) of GBCAs and a prolonged permanence of the drug in the body. NSF usually manifests itself approximately within 2–10 weeks after exposure to GBCAs. The United States Food and Drug Administration (FDA) issued a public health advisory in June 2006, recommending that GBCAs be used only if strictly necessary in patients with advanced kidney failure (Center for Drug Evaluation and Research, 2012).

More recently, the FDA issued an unexpected new safety note on GBCAs, reporting the risk for an occasional occurrence of Gd precipitates in the brain after repeated MRI procedures (Center for Drug Evaluation and Research, 2015). This risk of Gd precipitation has also been reported in pediatric patients (McDonald et al., 2017), who have a lifetime to manifest adverse clinical consequences (Roberts and Holden, 2016); however, so far these cases have not been clearly documented. This newly discovered condition is much less clear than NSF. In addition, reports have emerged over the last years regarding the accumulation of Gd in many tissues of subjects with normal renal conditions, including bone, brain and kidney (Di Gregorio et al., 2018; Rasschaert et al., 2018 2017; Robert et al., 2018). We and other authors have reported that some iron-related diseases in children are characterized by a long lasting Gd retention in the liver and kidney after single or multiple GBCAs administration (Maximova et al., 2016 2015). On November 2017, the European Medicines Agency (EMA) concluded its review of Gd deposition in brain and other tissues, recommending to restrict the use of some linear gadolinium agents used in MRI body scans and to suspend the authorisation of others (http://www.ema.europa.eu/ema/). This has important consequences for clinical practice.

GBCAs are stable Gd complexes, normally eliminated by the kidney through glomerular filtration within a few hours after injection, as suggested by the manufacturers, while their excretion is prolonged to several days in dialyzed patients or those with renal failure (Schuhmann-Giampieri and Krestin, 1991). In order to explain the mechanism of the NSF onset, it has been proposed that, during the prolonged permanence in the body, Gd dissociates from the ligand, leading to high levels of free Gd^{3+} ions which may readily bind other molecules and trigger the fibrogenic cascade (Morcos and Thomsen, 2008). The chemical stability of the complexes is thus crucially important in order to avoid Gd dissociation and its toxic effects (Morcos and Thomsen, 2008). The chemical configuration of GBCAs molecules can be divided into linear or cyclic, with the Gd ion “caged” in the cavity of the ligand: since cyclic molecules offer a stronger binding of Gd compared to the linear (Frenzel et al., 2008; Morcos and Thomsen, 2008), the former complexes are those more frequently used in hospitals after the NSF discovery (Mithal et al., 2017). Molecules of low stability are prone to undergo transmetalation with endogenous ions, particularly under acid conditions, leading to the release of free Gd^{3+} ions, which may then deposit in tissues and initiate the process of fibrosis. This is the possible trigger for NSF (Leiner et al., 2007) in patients with reduced renal elimination, favoured by a long permanence time in blood. Some authors suggest that free Gd ions directly affect cells of the skin and/or other tissues, accumulating probably in the lysosomes (Schuhmann-Giampieri and Krestin, 1991) and/or involving circulating fibrocytes (Okada et al., 2011).

Gadolinium deposition has been observed in the skin of NSF patients in many reports (Abraham et al., 2008). Boyd et al. (Boyd et al., 2007) have demonstrated the presence of Gd in areas of calcium phosphate deposition in blood vessels in a skin biopsy obtained from a patient with clinical features consistent with NSF after administration of gadodiamide. Most results have been obtained with scanning electron microscopy/energy dispersive X-ray spectroscopy (SEM/EDS)(Abraham and Thakral, 2008) and/or plasma mass spectrometry (ICP-MS) (Bernardi et al., 2011), that confirm a non-homogeneous deposition of Gd in the tissues, generally associated with other elements like Ca and P. As a result of these findings, recent synchrotron based XRF analyses including speciation studies have been reported (Sanyal et al., 2011). Findings indicate phosphate-bound Gd in skin in nephrogenic systemic fibrosis (George et al., 2010).

With the aim to better understand Gd precipitation in tissues and the role of GBCAs in the development of syndromes like NSF, experimental protocols were applied to animal models using normal rodents or rodents with 5/6 subtotal nephrectomy. The subtotal nephrectomy model was proposed to reproduce a comparable situation to that of patients with advanced chronic kidney disease (Morcos and Haylor, 2010; Wagner et al., 2012). However, a frequent bias in the reported studies with animals, although reproducing some NSF-like features, is that excessively high doses of Gd are used, thus complicating the translation to the patients. In this work we present a study performed in female mice with 5/6 subtotal nephrectomy and administration of two GBCAs at doses close to those used in clinics: two subsequent doses of 0.7 mmol/kg body weight. We compared two commercial MRI-CAs with linear cages: Gadodiamide (Omniscan®) which is the least stable contrast agent on the market and Gadopentetate dimeglumine (Magnevist®) widely used in the past and associated to NSF cases. We investigated the presence of Gd in the mice tissues (kidney, liver, femur, dorsal skin, teeth) one month after the administration of the last dose by using two synchrotron-based XRF microscopies at different spatial resolution: a macro system (SYRMEP beamline, Elettra synchrotron) to rapidly screen the Gd presence in explanted organs prone to accumulate Gd in NSF, and a micro-system (ID21 beamline, at the European Synchrotron Radiation Facility) to map the Gd at sub-cellular resolution, while monitoring also the distribution of other endogenous elements (Ca, Fe, P, S). Finally, LA-ICP-MS analyses were performed to confirm the findings.

2. Materials and methods

2.1. Chemicals and materials

The non-ionic linear chelate, Gd-DTPA-BMA (Omniscan®, GE Healthcare, USA) and the ionic linear molecule, Gd-DTPA (Magnevist®, Bayer Healthcare, Germany) are all approved and marketed products, and were purchased from their respective manufacturers. These compounds (250 mmol/L, respectively) are formulated as sterile and apirogenic aqueous solutions for injections without additional excipients. All other chemicals, unless otherwise specified, were purchased from Sigma-Aldrich (Milan, Italy).

2.2. Animals and GBCAs administration

Twenty one female CBA mice, weighing 20–25 g were used for the present study. The animals were housed in standard plastic cages at a constant temperature of 22 °C, with a 12-h light-dark cycle and ad libitum access to water and standard mouse diet. The colony was maintained specific-pathogen free in the animal house of the University of Trieste. All the experimental procedures were carried out in accordance with the Animal Care and Use guidelines of the ethics Committee of The University of Trieste. A 5/6 nephrectomy was performed at the animal house of the University of Trieste six weeks before the experiment. The 5/6 nephrectomy consists of the surgical excision of one kidney first, followed by the excision of two-third of the contralateral kidney. This procedure reproduces a renal failure condition in vivo (Bernardi et al., 2011). Female CBA mice were divided in two groups. The first 13 animals were 5/6 partial nephrectomised, while the remaining 8 animals were used as control and were operated but not nephrectomised (sham operated). Sixteen weeks after surgery, 18 animals (6 sham and 12 operated) were injected intravenously into the tail

Table 1
Animal treatment and clinical parameters. Urea and creatinine blood levels were measured in sham operated mice, 4, 6 and 14 weeks after 5/6 nephrectomy. The data are expressed as mean ± S.D. (mg/dl). In parenthesis the number of the animals in each experiment is given.

Treatment	4 weeks a.s.	6 weeks a.s.	14 weeks a.s.	16 weeks a.s.	20 weeks a.s.
Sham (8 animals)	Urea 43 ± 8 mg/ml Creatinine 0.41 ± 0.06 mg/ml (n = 8 animals)	n.d.	n.d.	*Administration* 2 animals = Saline 3 animals = Magnevist® 3 animals = Omniscan®	*XRF analyses* (2 animals) (3 animals) (3 animals)
Nephrectomy (13 animals)	Urea 74.5 ± 11 mg/ml ** Creatinine 0.52 ± 0.08 mg/ml (n = 7 animals)	Urea 78.75 ± 10.1 mg/ml *** Creatinine 0.51 ± 0.09 mg/ml (n = 5 animals)	Urea 83.5 ± 8.5 mg/ml *** Creatinine 0.63 ± 0.16 mg/ml * (n = 13 animals)	*Administration* 1 animal = Saline 6 animals = Magnevist® 6 animals = Omniscan®	*XRF analyses* (1 animal) (6 animals) (6 animals)

a.s. = After surgery; n.d. = not determined. Statistical analysis: Student t-test:***$p < 0.001$. **$p < 0.01$. *$p < 0.5$ vs. relevant controls.

vein with 2 doses of Omniscan® (0.7 mmol/kg body weight; in 3 sham and 6 operated mice) or Magnevist® (0.7 mmol/kg body weight; in 3 sham and 6 operated mice) every other day. Two mice sham and one operated received a saline isotonic (0.9%) solution. As reported in Table 1, creatinine and urea levels were monitored for each group four weeks after surgery and the day of the injection. The animals were sacrificed one month after the last injection and organs (kidney, liver, femur, dorsal skin, teeth) were explanted rapidly from carcasses, rinsed extensively with PBS, fixed in 10% formalin and stored at -20 °C until sectioning. From some animals injected with either Omniscan® (1 sham and 2 operated mice) or Magnevist® (1 sham and 2 operated mice), entire heads were obtained from decapitation and immediately fixed in 10% formalin. Fleshless skulls were embedded in methylmethacrylate resin and thinly sectioned to analyse the whole dental implants and related periodontal tissue (Arfelli et al., 1998).

The samples analysed at the SYRMEP beamline at the Elettra synchrotron light source, Trieste (Italy), were enclosed in appropriate plastic cages and cooled by a thermoelectric Peltier element during analyses (Delfino et al., 2011). Teeth samples were analysed at room temperature.

In parallel, single teeth (incisors) were also embedded in resin and sectioned to a thickness of 200 µm, in order to be used for microscopy and XRF analyses at the European Synchrotron Radiation Facility (ESRF), Grenoble (France). The same preparation was used for the heads, only at a thickness of 1–2 mm.

2.3. XRF analyses at SYRMEP (Elettra)

XRF spectra were gathered at the SYRMEP beamline (Arfelli et al., 1998) using a collimated 500 µm x 500 µm X-ray beam, monochromatised at 11 keV. A compact detection module equipped with a high-performance X-ray sensor was used as described previously (Delfino et al., 2011). This includes a 10-mm^2 'droplet type' Silicon Drift Detector (SDD) cooled by a Peltier element below 0 °C (Rosa et al., 2003). The fluorescence detection system has an energy resolution of 133 eV (FWHM) at the Mn Kα line (5.89 keV) and a peak-to-background ratio of approximately 800. A charge-coupled device (CCD) camera downstream the sample was used to monitor the beam-sample alignment as described previously (Delfino et al., 2011). A custom developed readout, control and acquisition unit (Alberti et al., 2008), specially designed for elemental mapping applications, allowed automatic mesh scans of selected areas with online data visualization, energy calibration and emission peak identification. The dwell time per point ranged from 30 to 60 s. Gadolinium detection is correlated with the L emission line energies at 6.08 and 6.7 keV, as previously tested under the present set-up (Delfino et al., 2011). The samples analysed at SYRMEP were enclosed in appropriate plastic cages, and were Peltier-cooled.

2.4. Microtomography set-up at SYRMEP

Incisors were imaged using the micro-tomography set-up available on SYRMEP. The imaging detector was a phosphorus fiber optic-coupled CCD (Photonic Science Ltd, X-ray Imager-VHR 60 camera system) with a pixel size of 10 µm and an effective spatial resolution of 18 µm full width at half maximum of the point spread function. The pixel depth was 12 bits. For each projection, four images with an exposure time of 2.5 s each were averaged, resulting in an overall exposure time per projection of 10 s (Dullin et al., 2017).

2.5. Micro-XRF elemental analysis at ID21

The micro-XRF element analysis was carried out at the ID 21 beamline of the ESRF using a set-up described earlier (Cotte et al., 2017). A 7.3-keV monochromatic X-ray beam was focused onto the sample, with a spot size of 2 × 0.9 μm^2 (VERT × HOR). The sample was mounted on a custom XYZ stage, rotated 30° away from the optical axis, and facing a 10 mm^2 Silicon Drift Diode (Röntec, Germany) placed 3.5 cm from the sample (Cotte et al., 2017). A photodiode was placed downstream the sample to collect the transmitted photons. Images were acquired by raster scanning the samples through the stationary beam. The step size ranged from 0.5 to 2 µm and the dwell time ranged from 0.4 to 1 s/ pixel.

2.6. LA-ICP-MS analyses

LA-ICP-MS measurements we performed on the same samples used for XRF analysis, using a 193 nm AF* excimer solid-state laser ablation system from New Wave Research (Cetac Analyte G2, Teledyne CETAC Technologies, Omaha, USA), interfaced with a quadrupole ICP-MS instrument (Agilent 7900, Agilent Technologies, Santa Clara, USA). The system was equipped with a HelEx 2-volume laser ablation cell, mounted on a motorized stage. Ablation parameters were as follows: laser energy density, 2.55 J cm^{-2}; repetition rate, 25 Hz; beam diameter, 10 µm; line scan speed, 20 µm s^{-1}; total acquisition time, 0.5 s (P-31, 0.1 s; Fe-57, 0.1 s; Gd-157, 0.291 s). The ablated material was transported from the ablation cell to the ICP using helium as a carrier gas. Argon was added as a make-up gas before the torch of the ICP. The ions formed in the ICP were extracted in the quadrupole mass spectrometer and separated according to their mass-to-charge ratios. The ICP-MS was set up in a time-resolved analysis mode, measuring one data point per spectral peak for the subsequent isotopes: ^{31}P, ^{56}Fe and ^{157}Gd. Data are reported in counts per second (cps).

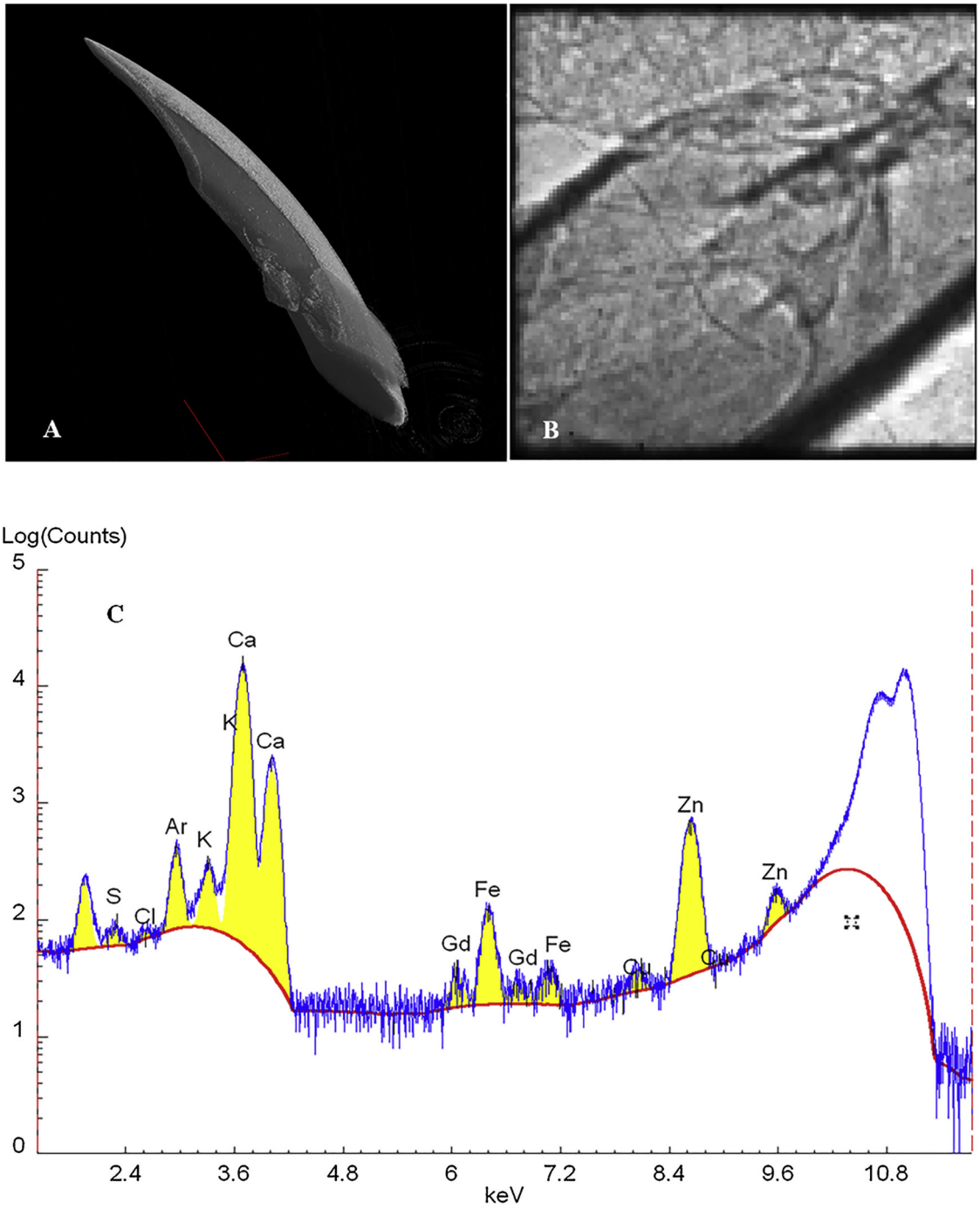

Fig. 1. Spectrum (Panel C) of a non-included incisor tooth of a 5/6 nephrectomised CBA mouse treated i.v. with two doses of Gd-DTPA-BMA (Omniscan®, GE Healthcare, USA) (0.7 mmol/kg body weight). The spectrum was acquired at the SYRMEP beamline at the Elettra Synchrotron light source (Trieste, Italy) with an X-ray beam energy of 11 keV, spot size of ca. 500 × 500 μm^2. The dwell time per point ranged from 30 to 60 s. Panel A: tomographic image of the tooth acquired at SYRMEP. Panel B: a phase contrast image of the tooth 1 × 1 mm^2, dwell time 500 s.

2.7. Software

For the data acquired at ID21, PyMCA (Solé et al., 2007), a free software package developed by the Data Analysis unit of the Software group of the ESRF, was used for processing and analysis of XRF spectra.

At Elettra, data acquisition was carried out using the PoliMiMCA software developed by Politecnico di Milano (Milan, Italy) while Matlab (The Math-Works, Natick,MA, USA) was used for data processing. Dark and flat field corrected data were reconstructed using the COBRA software code from EXXIM (http://www.exxim-cc.com/Index.htm). Slice data were analysed, manipulated and rendered using the Osirix software package (http://www.osirix-viewer.com) and ImageJ (http://rsb.info.nih.gov/ij/).

2.8. Statistical analysis for clinical parameters

Statistical analysis was carried out using analysis of variance combined with the Student's two-tailed t-test. Differences among the conditions were considered significant at $P < 0.05$.

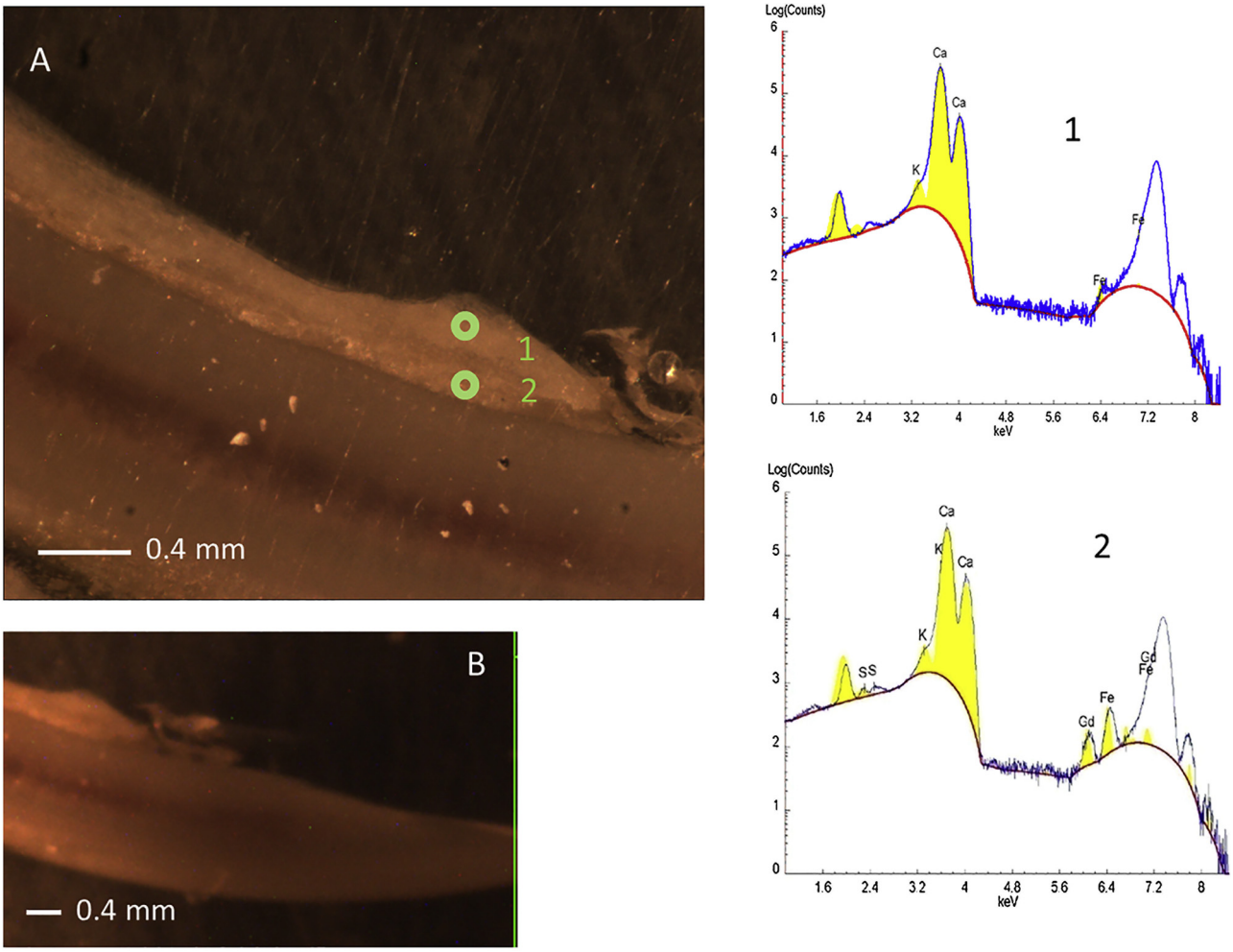

Fig. 2. A 200-μm thick section of a resin-embedded incisor tooth of a 5/6 nephrectomised CBA mouse one month after Omniscan® administration. The sample was analysed at the ID-21 ESRF beam line (Grenoble, France). At ID-21 the incident photon energy was set to 7.3 keV, and the beam was focused onto the sample by means of a W zone plate, on a spot of 0.2 × 0.9 μm^2 (VERT × HOR). In Panel A the entire optical image of the tooth is shown and in Panel B a detailed image of the region analysed, with spots 1 and 2 indicating the exact points of the acquisition of the spectra.

3. Results

3.1. Animal models of renal impairment and Gadolinium toxicity

The induction of renal failure was verified by measuring urea and creatinine blood levels after four, six and fourteen weeks following the 5/6 nephrectomy. Two weeks after the last assessment, the animals received the contrast agent by i.v. injection.

Table 1 reports the two clinical parameters at the different measurement times. While sham operated mice present a healthy renal status with a creatinine level of 0.41 ± 0.06 mg/dl and urea level of 43 ± 8 mg/dl, the 5/6 nephrectomised mice reveal an initial renal insufficiency four weeks after surgery, with a significant increase of urea blood concentration (74.5 ± 11 mg/dl). The insufficiency became severe at fourteen weeks (urea values: 83.5 ± 8.5 mg/dl). Intermediate values were recorded at 6 weeks after surgery. Significant renal damage was confirmed by creatinine plasma levels fourteen weeks after nephrectomy (0.63 ± 0.16 mg/dl* vs 0.41 ± 0.06 mg/dl).

Autoptic anatomical evaluation of the animals did not reveal any difference among the groups. In particular, no macroscopic changes of the skin were observed in any of the treated animals. Only at the injection site a generic sign of injury was revealed. This may indicate that the administered drug doses were insufficient to produce an overt NSF-like syndrome.

3.2. Macro XRF elemental analysis at 11 keV energy

In order to reveal possible traces of Gd, all the explanted tissues were analysed under the XRF set-up of the SYRMEP beamline at 11 keV photon energy. Averaged spectra (10 spectra per sample) were collected at different points (spot area: 1 × 1 mm^2) of liver, skin, vessels, kidney, femur and teeth, from every animal group (Table 1). Gadolinium levels were found to be below the detection limit (a few ppm) in all the tissues of the 6 animals with normal renal function (sham operated animals) that received the contrast agent(s). Similarly, XRF analyses of all the tissue samples related to the 12 animals receiving the contrast agents and with 5/6 nephrectomy showed no detectable presence of Gd with the exception of teeth. Surprisingly, a clear presence of this element was evident in the incisors, particularly at the radical extremities of nephrectomised mice treated with GBCAs.

Fig. 1 shows images and the XRF spectra collected on a fixed incisor from a mouse injected with Omniscan; in detail, Panel A shows a section of the tomographic image; panel B reports a phase contrast image of a 1 × 1mm^2 close-up on the same tooth, in an area where Gd was detected; panel C shows the XRF spectrum acquired from the region in panel B at 11.0 KeV, with a spot size of 1 × 1 mm^2 and an acquisition time of 500 s. Gd is clearly revealed by the two peaks at 6.07 and 6.7 keV, corresponding to its L emission lines. Similar data were obtained with the incisors of nephrectomised mice treated with Magnevist.

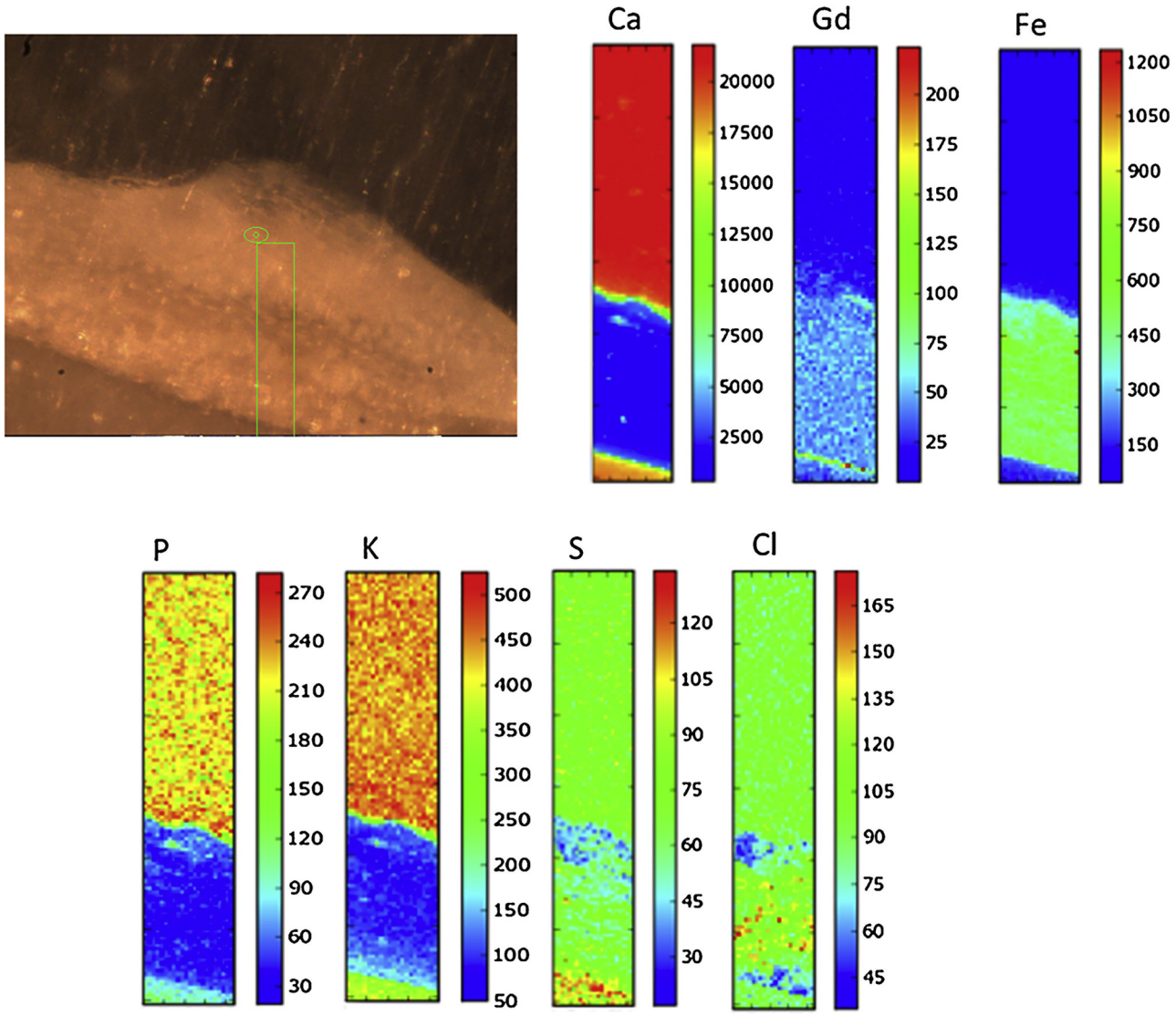

Fig. 3. Micro elemental mapping of a 200-μm thick section of a resin-embedded incisor tooth of a 5/6 nephrectomised CBA mouse treated with Omniscan®. Elemental scans were made at the ID-21 ESRF beam line (Grenoble, France) with a 7.3 keV X-ray beam energy. An optical image (panel A) of the bone matrix and periodontal periodontal tissue of the tooth is shown next to element maps of P, Ca, S, Gd, Fe, Cl and K. The step size was 2 μm and the dwell time was set to 2 s/pixel.

3.3. Micro XRF elemental analysis in histological tooth tissue specimens

In order to precisely localize Gd in tooth samples, we performed XRF spectroscopy and elemental imaging of tissues embedded in resin (see Materials and Methods) at the ID-21 beamline, with a 7.3 keV beam incident energy. Histological sections of liver, kidney and skin of all the animal groups were also analysed, but again Gd was below the detection limit of the technique. Due to the negative results obtained by macro XRF, together with the difficulty in obtaining adequate histological sections from these tissues, femurs were not analysed further with this set-up.

In Fig. 2, a 200-μm thick section of the tooth of Fig. 1 is imaged (panels A and B): the periodontal ligament is clearly visible as attached to the cementum of the tooth.

Several spectra were collected in different regions of the sample with a 4 μm^2 spot size. Most of the tissue showed no signs of Gd presence, although variable amounts of Ca, P, Fe and S were found, depending on its structure. Panels 1 and 2 show the spectra corresponding to the respective points indicated in panel B, collected in the periodontal ligament. Gadolinium seems undetectable in the alveolar bone side of the ligament (panel 1), but shows up in the cementum side of the tissue (panel 2). Fig. 3 shows the results of the XRF elemental maps obtained by raster scanning a region of the incisor in Fig. 2, close to the analysed points. The exact region is shown as a visible light micrograph in Fig. 3, panel A. The elemental maps of P, S and Ca appear to correlate with the extent of calcification in the different tissue portions: Ca and P are characteristic elements of calcified tissues, and thus allow to clearly distinguish between the bone structure of the tooth and the bone. The low levels of Ca and P, together with a high abundance of S, identifies accurately the periodontal ligament close to the cementum (low side). The ligament region displays a high S content, as expected from collagen presence, and abundance of Fe, associated with high vascularization. Gadolinium is clearly present in all the periodontal ligament, but predominantly concentrated in a thin line on the edge of the periodontal tissue near the cementum of the tooth, where S is also at its highest levels. Similar elemental patterns, including Gd presence, have been found in the teeth from the nephrectomised animals injected with Magnevist. The Gd distribution is generally suggestive of a maximal accumulation in the cell layer lining the cementum, while no hot-spots (suggestive of aggregates) are revealed (Schroeder et al., 2008). At the same time no histological changes have been noticed in the periodontal ligament samples.

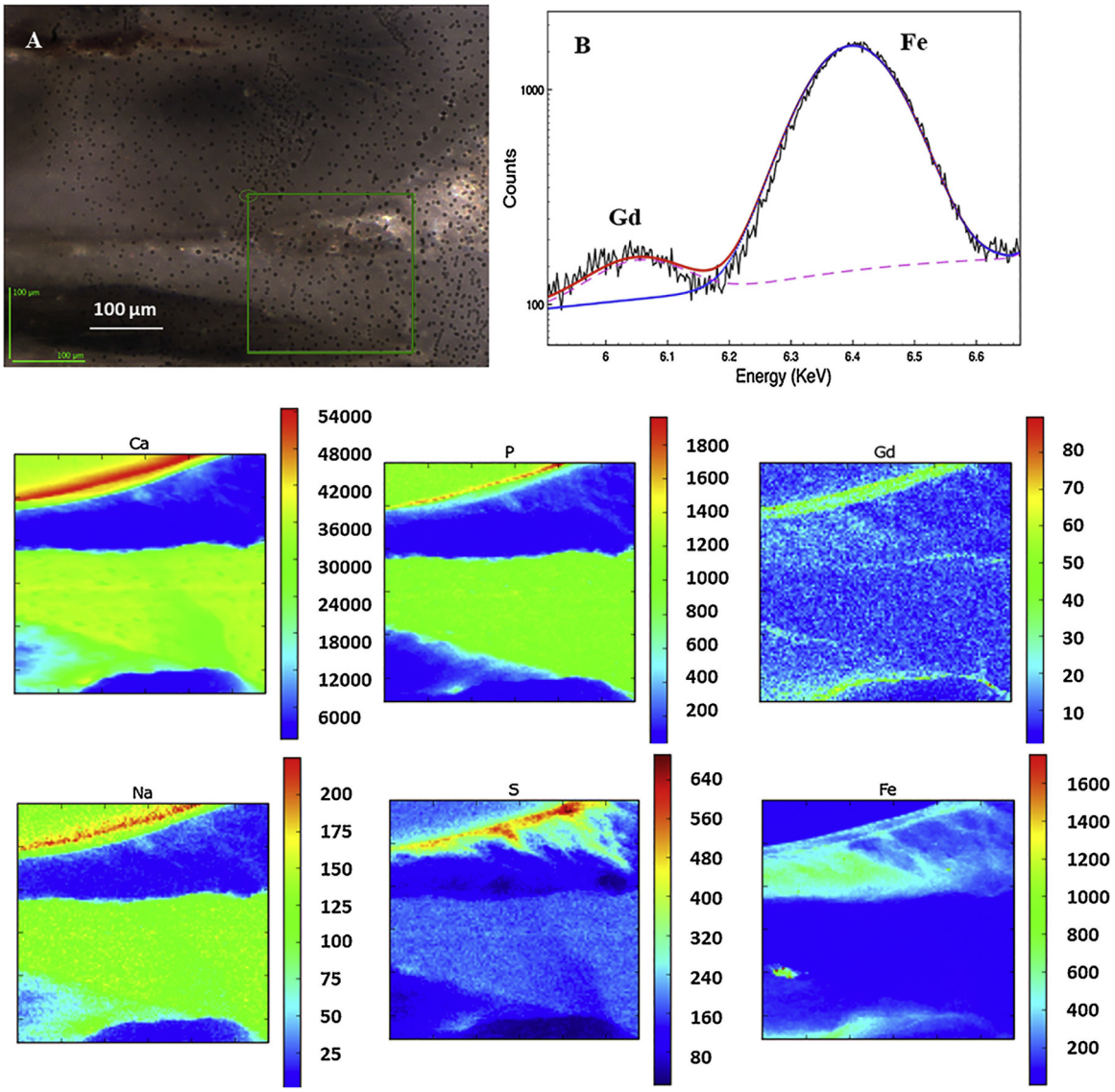

Fig. 4. Micro elemental mapping at ID-21 with a 7.3 keV X-ray beam energy of a 2-mm thick skull section from a 5/6 nephrectomised CBA mouse treated with Magnevist®. The optical image (panel A) and detail of the spectrum (panel B) of the bone matrix and periodontal tissue of the tooth are shown, next to elemental maps of Ca, P, Gd, Na, S and Fe. The step size was 2 µm and the dwell time was set to 2 s/pixel.

The same analytical protocol was also followed for skull histological samples containing periodontal tissues. The sample in Fig. 4 is from a nephrectomised mouse injected with Magnevist®. The optical micrograph (Fig. 4, panel A) shows a tooth with surrounding periodontal ligament and alveolar bone (arrows). As in Fig. 3, the Gd presence is associated again with the periodontal ligaments, but not the bone. In panel B the spectrum of a small region inside the analysed area shows the specific presence of Gd in the densest periodontal region (box in the Gd map): in the XRF spectrum the peak of gadolinium around 6.057 keV is clearly resolved from that of Fe. The reported elemental maps confirm the presence of Gd in good correlation with Fe and S, as seen before in Fig. 3. In the lower part of the images, some Fe, Gd and S does not seem to correlate with the optical image. These XRF signals most probably derive from internal structures instead of the visible surface. In Fig. 5 a similar sample is shown, but in this case the localization of Gd is resolved in periodontal ligament at the alveolar bone side, from a mouse administered with Omniscan®. This figure demonstrates that Gd is also abundant in the thin cell layer lining of the ligament at the alveolar bone side.

A tissue slice showing the dental implant in the jaw from a sham operated mouse injected with Omniscan is shown in Figure S1. The maps indicate that there is no Gd accumulation in this animal as the count level is low, and there are no evident Gd hot spots. Similar results were obtained for the sham operated animals receiving Magnevist® (data not shown).

3.4. *LA-ICP-MS analyses on skull slices*

To finally confirm the presence of Gd in the periodontal ligament with a different chemical principle, excluding the low chemical sensitivity of XRF, technical artefacts and/or misinterpretations (Gholap et al., 2010; Trejos et al., 2013), we performed LA-ICP-MS analysis on some skull slices of treated animals. Fig. 6 shows representative results for nephrectomised animals who received Omniscan®. Similar to XRF mapping, P identifies the calcified material, while Fe is localized in the periodontal tissue where Gd is confirmed to be present.

4. Discussion

In this study we report evidence of long lasting retention of Gd in a

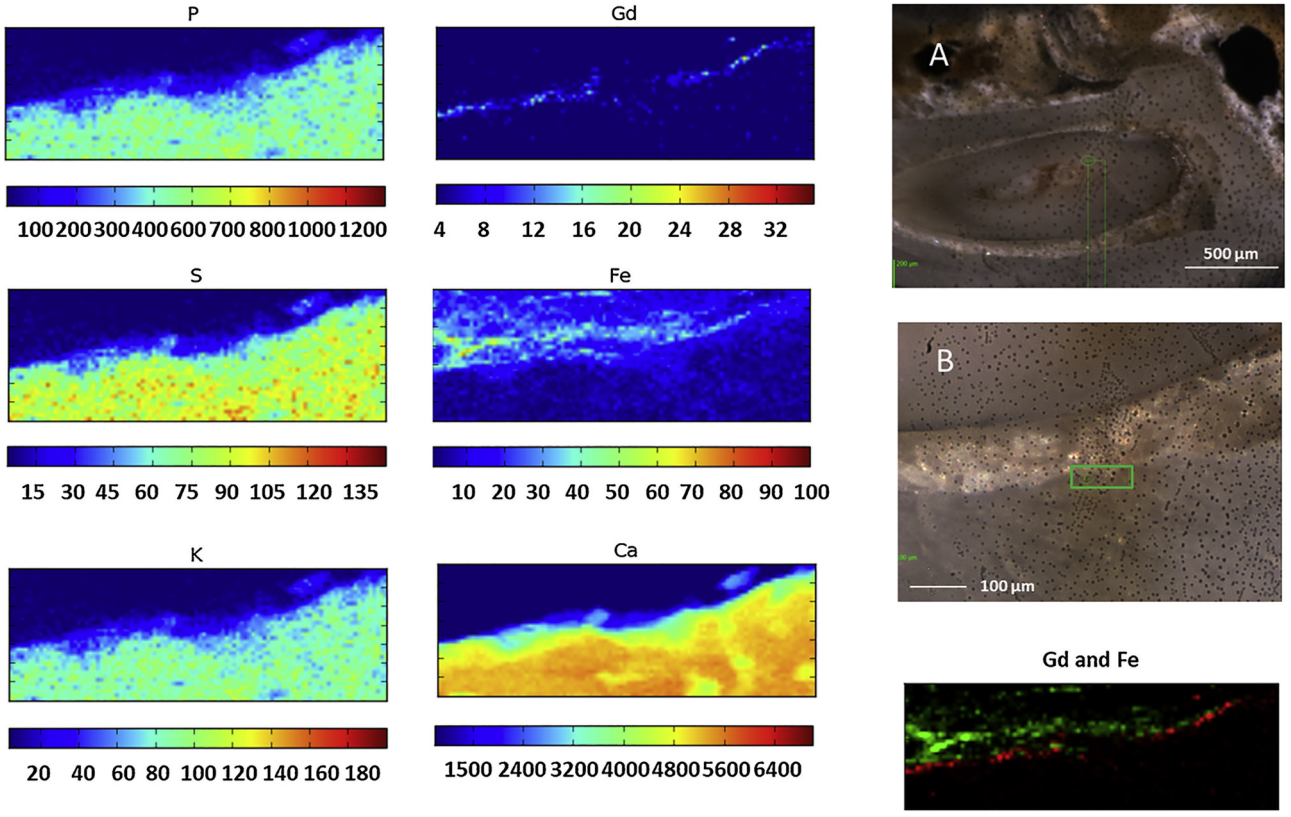

Fig. 5. Micro elemental mapping at ID-21 with a 7.3 keV X-ray beam energy of a 2-mm thick scull section of a 5/6 nephrectomised CBA mouse injected with Omniscan®. Panels A and B are light images at increasing magnification of the sample. In panel B, the green box indicates the analysis sub-region. Other panels are single element maps and one shows the colocalization of Gd and Fe.
The step size was 2 µm and the dwell time was set to 2 s/pixel.

body district never reported before, which is the periodontal tissue in a murine model of renal impairment. We administered two linear GBCAs at two closely repeated doses to a model of partially nephrectomised mice. The residual presence of Gd detected was clearly linked to the condition of renal impairment that causes a slow drug excretion and favours an incomplete elimination from the mouse body. Different from others studies employing GBCAs in healthy (Pietsch et al., 2011; Sieber et al., 2008a 2008b) or 5/6 nephrectomised mice (Grant et al., 2009; Haylor et al., 2010) to reproduce the NSF condition, we did not find any skin lesion related to the pathology, probably because the Gd dosages we used were far lower than the reported ones. It is also possible that the development of NSF in the mice requires a time span larger than the one we employed. Despite failing in reproducing the NSF symptoms, we found novel results that may lead to a better understanding of the GBCAs toxicity, not only in relation to development of NSF.

To reveal the Gd presence we used Synchrotron XRF fluorescence at two different beamlines, allowing us to explore two complementary dimensional scales. XRF with the millimetre beam approach had the main advantage of rapid screening of many tissues (kidney, liver, femur, dorsal skin, teeth), as previously demonstrated (Delfino et al., 2011), albeit with moderate sensitivity. Gd was seemingly detected only in tissues with a concentration higher than 10 ppm. When performed under microscopy set-up, thanks to the penetration of the beam, synchrotron XRF analyses are clearly superior to the common surface elemental analyses (such as SEM-EDS) (Sanyal et al., 2011). The elemental mapping obtained by XRF microscopy allowed us to compare the Gd distribution with that of other endogenous elements such as Fe, Ca and P, as demonstrated previously (Delfino et al., 2011). The distribution and extreme abundance of Ca and P in our samples allowed us to clearly recognize bone and tooth structures, while high S and Fe were indicative of periodontal tissues. Gadolinium is accumulated in this membrane-like tissue surrounding the tooth and it seems to co-localize with the amino-acidic sulphur of collagen fibres. Interestingly, elemental mapping reveals that in this tissue the abundant Fe partially co-localizes with Gd. A relationship between Fe and GBCA toxicity has been recently proposed, suggesting the involvement of ferroportin expressing cells (macrophages and fibrocytes) in the deposition of Gd in NSF affected tissues, as well as in the globus pallidus, thalamus, caudate nucleus, and dentate nucleus of brain (Swaminathan, 2016). GBCAs seem to induce CD163, ferroportin and macrophages that are the likely sources of tissue iron accumulation seen in NSF patients. In other studies, Gd has been shown to perturb cellular iron metabolism in macrophages, since the addition of linear GBCM dramatically increased transferrin-dependent cellular iron uptake and induced an increase in H-ferritin content (Ghio et al., 2011). Altogether, there are findings indicating that both heme- and non-heme iron import, storage and export pathways are activated by GBCAs. Further investigations are desirable to determine whether the Gd deposition we found in the periodontal ligament is actually linked to Fe metabolism. The periodontal ligament is a membrane-like connective tissue surrounding the root of a tooth. It lies between the hard tissues of alveolar bone and cementum of teeth and serves to anchor the tooth to the alveolus. This ligament is very rich in collagen type I and IV fibres and fibronectin. In particular, collagen type I is predominantly present in periodontal ligament, forming compact fibres anchored to cementum and to the alveolar bone. Collagen type IV is also localized in basal membranes of vessels. This may be an interesting link with NSF pathology since Gd (particularly in skin) has been found frequently on the wall of microvessels (Sanyal et al., 2011). In the skin of NSF biopsies, a significant increase of collagen is observed and, in some cases, deposits of mucin are reported: mucins are also abundant in the periodontal tissue. However, the most important connection between periodontal tissue

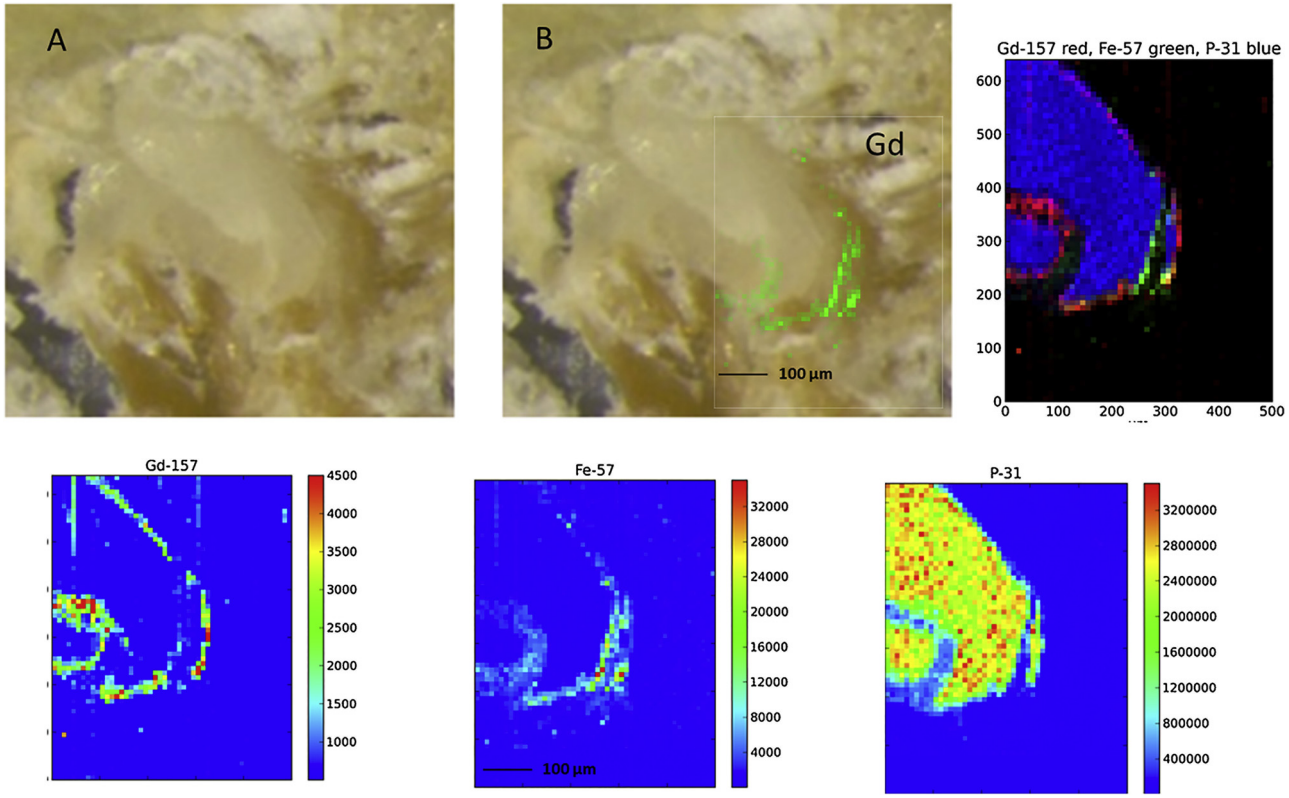

Fig. 6. LA-ICP-MS mapping on a skull section from an Omniscan® treated and nephrectomised mouse. Panel A and B are light images of the sample, while in B the Gd localization is superimposed.
Gadolinium, P and Fe mapping of the tissue samples have been obtained on a virtual mapping grid with a grid size of 10 µm and a map size of ca.1.0 mm × 0.75 mm using the so-called line of spots method, where consecutive parallel lines were ablated.

and NSF features may be that in NSF, at tissue level, fibrotic lesions are accompanied by an increased presence of fibroblast-like cells, dermal macrophages, and fibrocytes. Periodontal tissue is a connective tissue undergoing rapid remodelling, especially in rodents, and contains many types of fibroblasts and frequent fibrocytes (Deporter et al., 1984).

The periodontal ligament in rodents is a repository for cells involved in the formation of the cementum, the periodontal ligament itself and the alveolar bone. Since periodontal tissue of mice is a continuously regenerating region, our results could also suggest that contrast agents have a tropism for organs and tissues (such as skin) with rapid renewal processes; moreover, among the various body tissues, the skin is one that has a structure similar to that of periodontal ligament.

Our XRF analyses suggest that the borders of this tissue, in close contact with the tooth, are the areas maximally accumulating Gd. This is particularly evident in Figures 3, 4 and 5, and confirmed by LA-ICP-MS measurements. Interestingly, in contrast with reports on NSF and Gd deposition in brain, we found no co-localization with Ca and P. It could be speculated that XRF allows a superior chemical specificity, or that there are no calcified precipitates, but perhaps an intracellular accumulation. Mainstream reports advocate that Gd transmetallation in tissues produces free Gd^{3+} ions that immediately combine with anions such as phosphate to form $GdP0_4$ salts, or with some other chemical species. Our data do not exclude these findings. Moreover, histological examination of the samples did not evidence cellular changes related to administration of GBCAs and Gd accumulation.

We did not note a difference between the two contrast agents although they have a different chemical structure. However, in order to verify if the molecular arrangement influences periodontal deposition, additional studies will be necessary including other drugs and particularly the cyclic GBCAs. Furthermore, our methods cannot unravel the chemical speciation of Gd that would represent the next step in this research.

Additionally, our study is associated with some limitations related to rather high limits of detection for XRF (a few tens of ppm) associated with Gd-L_3 lines, hence this low chemical sensitivity limits comprehensive detection of Gd at the whole body level. For this reason we may have missed Gd retention sites in other body parts.

5. Conclusions

In summary, we showed that in a murine model of renal impairment, high Gd-CA doses produce a deposition of Gd in the periodontal tissue. We believe that these findings may have important implications in the understanding of NSF pathology. If further confirmed, periodontal tissue may represent a new cellular site for both investigations and diagnostic purposes.

Transparency document

The Transparency document associated with this article can be found in the online version.

Acknowledgment

This work was partially supported by the Institute for Maternal and Child Health IRCCS Burlo Garofolo (Trieste, Italy). The authors thank Dr. Fulvio Stacul for helpful scientific suggestions. The authors are grateful to the ESRF and Elettra Synchrotrons for granting the beamtimes (MD375, MD462 and 20085358, respectively).

References

Abraham, J.L., Thakral, C., 2008. Tissue distribution and kinetics of gadolinium and nephrogenic systemic fibrosis. Eur. J. Radiol. 66, 200–207. https://doi.org/10.1016/j.ejrad.2008.01.026.

Abraham, J.L., Thakral, C., Skov, L., Rossen, K., Marckmann, P., 2008. Dermal inorganic gadolinium concentrations: evidence for in vivo transmetallation and long-term persistence in nephrogenic systemic fibrosis. Br. J. Dermatol. 158, 273–280. https://doi.org/10.1111/j.1365-2133.2007.08335.x.

Alberti, R., Guazzoni, C., Klatka, T., 2008. USB 2.0 data acquisition system for high-speed X-ray elemental mapping. J. Instrum. 3https://doi.org/10.1088/1748-0221/3/03/P03003. P03003–P03003.

Arfelli, F., Assante, M., Bonvicini, V., Bravin, A., Cantatore, G., Castelli, E., Dalla Palma, L., Di Michiel, M., Longo, R., Olivo, A., Pani, S., Pontoni, D., Poropat, P., Prest, M., Rashevsky, A., Tromba, G., Vacchi, A., Vallazza, E., Zanconati, F., 1998. Low-dose phase contrast x-ray medical imaging. Phys. Med. Biol. 43, 2845–2852. https://doi.org/10.1088/0031-9155/43/10/013.

Bernardi, S., Candido, R., Toffoli, B., Carretta, R., Fabris, B., 2011. Prevention of accelerated atherosclerosis by AT1 receptor blockade in experimental renal failure. Nephrol. Dial. Transplant. 26, 832–838. https://doi.org/10.1093/ndt/gfq524.

Boyd, A.S., Zic, J.A., Abraham, J.L., 2007. Gadolinium deposition in nephrogenic fibrosing dermopathy. J. Am. Acad. Dermatol. 56, 27–30. https://doi.org/10.1016/j.jaad.2006.10.048.

Center for Drug Evaluation and Research, 2015. Drug Safety and Availability - FDA Drug Safety Communication: FDA Evaluating the Risk of Brain Deposits With Repeated Use of Gadolinium-Based Contrast Agents For Magnetic Resonance Imaging (MRI). pp. 4–6.

Center for Drug Evaluation and Research, 2012. Postmarket Drug Safety Information for Patients and Providers - Information on Heparin [WWW Document]. URL. (Accessed 5.13.18). http://wayback.archive-it.org/7993/20161022053248/http://www.fda.gov/Drugs/DrugSafety/PostmarketDrugSafetyInformationforPatientsandProviders/ucm142882.htm.

Cotte, M., Pouyet, E., Salomé, M., Rivard, C., De Nolf, W., Castillo-Michel, H., Fabris, T., Monico, L., Janssens, K., Wang, T., Sciau, P., Verger, L., Cormier, L., Dargaud, O., Brun, E., Bugnazet, D., Fayard, B., Hesse, B., Pradas del Real, A.E., Veronesi, G., Langlois, J., Balcar, N., Vandenberghe, Y., Solé, V.A., Kieffer, J., Barrett, R., Cohen, C., Cornu, C., Baker, R., Gagliardini, E., Papillon, E., Susini, J., 2017. The ID21 X-ray and infrared microscopy beamline at the ESRF: status and recent applications to artistic materials. J. Anal. At. Spectrom. 32, 477–493. https://doi.org/10.1039/C6JA00356G.

Cowper, S.E., Kuo, P.H., Bucala, R., 2007. Nephrogenic systemic fibrosis and gadolinium exposure: association and lessons for idiopathic fibrosing disorders. Arthritis Rheum. 56, 3173–3175. https://doi.org/10.1002/art.22926.

Cowper, S.E., Robin, H.S., Steinberg, S.M., Su, L.D., Gupta, S., LeBoit, P.E., 2000. Scleromyxoedema-like cutaneous diseases in renal-dialysis patients. Lancet 356, 1000–1001. https://doi.org/10.1016/S0140-6736(00)02694-5.

Delfino, R., Altissimo, M., Menk, R.H., Alberti, R., Klatka, T., Frizzi, T., Longoni, A., Salomè, M., Tromba, G., Arfelli, F., Clai, M., Vaccari, L., Lorusso, V., Tiribelli, C., Pascolo, L., 2011. X-ray fluorescence elemental mapping and microscopy to follow hepatic disposition of a Gd-based magnetic resonance imaging contrast agent. Clin. Exp. Pharmacol. Physiol. 38, 834–845. https://doi.org/10.1111/j.1440-1681.2011.05618.x.

Deporter, D.A., Svoboda, E.L.A., Howley, T.P., Shiga, A., 1984. A quantitative comparison of collagen phagocytosis in periodontal ligament and transseptal ligament of the rat periodontium. Am. J. Orthod. 85, 519–522. https://doi.org/10.1016/0002-9416(84)90092-7.

Di Gregorio, E., Iani, R., Ferrauto, G., Nuzzi, R., Aime, S., Gianolio, E., 2018. Gd accumulation in tissues of healthy mice upon repeated administrations of Gadodiamide and Gadoteridol. J. Trace Elem. Med. Biol. 48, 239–245. https://doi.org/10.1016/j.jtemb.2018.04.018.

Dullin, C., Ufartes, R., Larsson, E., Martin, S., Lazzarini, M., Tromba, G., Missbach-Guentner, J., Pinkert-Leetsch, D., Katschinski, D.M., Alves, F., 2017. µCT of ex-vivo stained mouse hearts and embryos enables a precise match between 3D virtual histology, classical histology and immunochemistry. PLoS One 12, e0170597. https://doi.org/10.1371/journal.pone.0170597.

Frenzel, T., Lengsfeld, P., Schirmer, H., Hütter, J., Weinmann, H.J., 2008. Stability of gadolinium-based magnetic resonance imaging contrast agents in human serum at 37°C. Invest. Radiol. 43, 817–828. https://doi.org/10.1097/RLI.0b013e3181852171.

Galan, A., Cowper, S.E., Bucala, R., 2006. Nephrogenic systemic fibrosis (nephrogenic fibrosing dermopathy). Curr. Opin. Rheumatol. 18 (6), 614–617. https://doi.org/10.1097/01.bor.0000245725.94887.8d.

George, S.J., Webb, S.M., Abraham, J.L., Cramer, S.P., 2010. Synchrotron X-ray analyses demonstrate phosphate-bound gadolinium in skin in nephrogenic systemic fibrosis. Br. J. Dermatol. 163, 1077–1081. https://doi.org/10.1111/j.1365-2133.2010.09918.x.

Ghio, A.J., Soukup, J.M., Dailey, L.A., Richards, J., Deng, Z., Abraham, J.L., 2011. Gadolinium exposure disrupts iron homeostasis in cultured cells. J. Biol. Inorg. Chem. 16, 567–575. https://doi.org/10.1007/s00775-011-0757-z.

Gholap, D.S., Izmer, A., De Samber, B., van Elteren, J.T., Šelih, V.S., Evens, R., De Schamphelaere, K., Janssen, C., Balcaen, L., Lindemann, I., Vincze, L., Vanhaecke, F., 2010. Comparison of laser ablation-inductively coupled plasma-mass spectrometry and micro-X-ray fluorescence spectrometry for elemental imaging in Daphnia magna. Anal. Chim. Acta 664, 19–26. https://doi.org/10.1016/j.aca.2010.01.052.

Grant, D., Johnsen, H., Juelsrud, A., Lvhaug, D., 2009. Effects of gadolinium contrast agents in naive and nephrectomized rats: relevance to nephrogenic systemic fibrosis. Acta Radiol. 50, 156–169. https://doi.org/10.1080/02841850802637808.

Haylor, J., Dencausse, A., Vickers, M., Nutter, F., Jestin, G., Slater, D., Idee, J.M., Morcos, S., 2010. Nephrogenic gadolinium biodistribution and skin cellularity following a single injection of omniscan in the rat. Invest. Radiol. 45, 507–512. https://doi.org/10.1097/RLI.0b013e3181eb51f2.

Leiner, T., Herborn, C.U., Goyen, M., 2007. Nephrogenic systemic fibrosis is not exclusively associated with gadodiamide. Eur. Radiol. 17, 1921–1923. https://doi.org/10.1007/s00330-007-0663-5.

Maximova, N., Gregori, M., Zennaro, F., Sonzogni, A., Simeone, R., Zanon, D., 2016. Hepatic gadolinium deposition and reversibility after contrast agent-enhanced MR imaging of pediatric hematopoietic stem cell transplant recipients. Radiology 281, 152846. https://doi.org/10.1148/radiol.2016152846.

Maximova, N., Zanon, D., Pascolo, L., Zennaro, F., Gregori, M., Grosso, D., Sonzogni, A., 2015. Metal accumulation in the renal cortex of a pediatric patient with sickle cell disease: a case report and review of the literature. J. Pediatr. Hematol. Oncol. 37 (4), 311–314. https://doi.org/10.1097/MPH.0000000000000322.

McDonald, J.S., McDonald, R.J., Jentoft, M.E., Paolini, M.A., Murray, D.L., Kallmes, D.F., Eckel, L.J., 2017. Intracranial gadolinium deposition following gadodiamide-enhanced magnetic resonance imaging in pediatric patients: a case-control study. JAMA Pediatr. 171 (7), 705–707. https://doi.org/10.1001/jamapediatrics.2017.0264.

Mithal, L.B., Patel, P.S., Mithal, D., Palac, H.L., Rozenfeld, M.N., 2017. Use of gadolinium-based magnetic resonance imaging contrast agents and awareness of brain gadolinium deposition among pediatric providers in North America. Pediatr. Radiol. 47, 657–664. https://doi.org/10.1007/s00247-017-3810-4.

Morcos, S.K., Haylor, J., 2010. Pathophysiology of nephrogenic systemic fibrosis: a review of experimental data. World J. Radiol. 2, 427–433. https://doi.org/10.4329/wjr.v2.i11.427.

Morcos, S.K., Thomsen, H.S., 2008. Nephrogenic systemic fibrosis: more questions and some answers. Nephron - Clin. Pract. 110 (1), 24–31. https://doi.org/10.1159/000151228.

Okada, E., Yamanaka, M., Ishikawa, O., 2011. New insights into the mechanism of abnormal calcification in nephrogenic systemic fibrosis - gadolinium promotes calcium deposition of mesenchymal stem cells and dermal fibroblasts. J. Dermatol. Sci. 62, 58–63. https://doi.org/10.1016/j.jdermsci.2011.01.009.

Pietsch, H., Raschke, M., Ellinger-Ziegelbauer, H., Jost, G., Walter, J., Frenzel, T., Lenhard, D., H??tter, J., Sieber, M.A., 2011. The role of residual gadolinium in the induction of nephrogenic systemic fibrosis-like skin lesions in rats. Invest. Radiol. 46, 48–56. https://doi.org/10.1097/RLI.0b013e3181efd49a.

Rasschaert, M., Emerit, A., Fretellier, N., Factor, C., Robert, P., Idée, J.-M., Corot, C., 2018. Gadolinium retention, brain T1 hyperintensity, and endogenous metals: a comparative study of macrocyclic versus linear gadolinium chelates in renally sensitized rats. Invest. Radiol. 53, 328–337. https://doi.org/10.1097/RLI.0000000000000447.

Rasschaert, M., Idée, J.M., Robert, P., Fretellier, N., Vives, V., Violas, X., Ballet, S., Corot, C., 2017. Moderate renal failure accentuates T1 signal enhancement in the deep cerebellar nuclei of gadodiamide-treated rats. Invest. Radiol. 52, 255–264. https://doi.org/10.1097/RLI.0000000000000339.

Robert, P., Frenzel, T., Factor, C., Jost, G., Rasschaert, M., Schuetz, G., Fretellier, N., Boyken, J., Idée, J.-M., Pietsch, H., 2018. Methodological aspects for preclinical evaluation of gadolinium presence in brain tissue. Invest. Radiol. 53, 1. https://doi.org/10.1097/RLI.0000000000000467.

Roberts, D.R., Holden, K.R., 2016. Progressive increase of T1 signal intensity in the dentate nucleus and globus pallidus on unenhanced T1-weighted MR images in the pediatric brain exposed to multiple doses of gadolinium contrast. Brain Dev. 38, 331–336. https://doi.org/10.1016/j.braindev.2015.08.009.

Rosa, E.V.C., Valgas, C., Souza-Sierra, M.M., Corrêa, A.X.R., Radetski, C.M., 2003. Biomass growth, micronucleus induction, and antioxidant stress enzyme responses in Vicia faba exposed to cadmium in solution. Environ. Toxicol. Chem. 22, 645–649.

Sanyal, S., Marckmann, P., Scherer, S., Abraham, J.L., 2011. Multiorgan gadolinium (Gd) deposition and fibrosis in a patient with nephrogenic systemic fibrosis - an autopsy-based review. Nephrol. Dial. Transplant. 26, 3616–3626. https://doi.org/10.1093/ndt/gfr085.

Schroeder, J.A., Weingart, C., Coras, B., Hausser, I., Reinhold, S., Mack, M., Seybold, V., Vogt, T., Banas, B., Hofstaedter, F., Krämer, B.K., 2008. Ultrastructural evidence of dermal gadolinium deposits in a patient with nephrogenic systemic fibrosis and end-stage renal disease. Clin. J. Am. Soc. Nephrol. 3, 968–975. https://doi.org/10.2215/CJN.00100108.

Schuhmann-Giampieri, G., Krestin, G., 1991. Pharmacokinetics of Gd-DTPA in patients with chronic renal failure. Invest. Radiol. 26, 975–979.

Sieber, M.A., Lengsfeld, P., Frenzel, T., Golfier, S., Schmitt-Willich, H., Siegmund, F., Walter, J., Weinmann, H.J., Pietsch, H., 2008a. Preclinical investigation to compare different gadolinium-based contrast agents regarding their propensity to release gadolinium in vivo and to trigger nephrogenic systemic fibrosis-like lesions. Eur. Radiol. 18, 2164–2173. https://doi.org/10.1007/s00330-008-0977-y.

Sieber, M.A., Pietsch, H., Walter, J., Haider, W., Frenzel, T., Weinmann, H.J., 2008b. A preclinical study to investigate the development of nephrogenic systemic fibrosis: a possible role for gadolinium-based contrast media. Invest. Radiol. 43, 65–75. https://doi.org/10.1097/RLI.0b013e31815e6277.

Solé, V.A.A., Papillon, E., Cotte, M., Walter, P., Susini, J., 2007. A multiplatform code for the analysis of energy-dispersive X-ray fluorescence spectra. Spectrochim. Acta - Part B At. Spectrosc. 62, 63–68. https://doi.org/10.1016/j.sab.2006.12.002.

Swaminathan, S., 2016. Gadolinium toxicity: iron and ferroportin as central targets. Magn. Reson. Imaging 34, 1373–1376. https://doi.org/10.1016/j.mri.2016.08.016.

Tedeschi, E., Caranci, F., Giordano, F., Angelini, V., Cocozza, S., Brunetti, A., 2017. Gadolinium retention in the body: what we know and what we can do. Radiol. Medica. 122 (8), 589–600. https://doi.org/10.1007/s11547-017-0757-3.

Trejos, T., Koons, R., Becker, S., Berman, T., Buscaglia, J., Duecking, M., Eckert-Lumsdon, T., Ernst, T., Hanlon, C., Heydon, A., Mooney, K., Nelson, R., Olsson, K., Palenik, C., Pollock, E.C., Rudell, D., Ryland, S., Tarifa, A., Valadez, M., Weis, P., Almirall, J., 2013. Cross-validation and evaluation of the performance of methods for the elemental analysis of forensic glass by μ-XRF, ICP-MS, and LA-ICP-MS. Anal. Bioanal. Chem. 405, 5393–5409. https://doi.org/10.1007/s00216-013-6978-y.

Wagner, B., Tan, C., Barnes, J.L., Ahuja, S., Davis, T.L., Gorin, Y., Jimenez, F., 2012. Nephrogenic systemic fibrosis: evidence for oxidative stress and bone marrow-derived fibrocytes in skin, liver, and heart lesions using a 5/6 nephrectomy rodent model. Am. J. Pathol. 181, 1941–1952. https://doi.org/10.1016/j.ajpath.2012.08.026.